High-order harmonic generation from C_{60}-rich plasma

R. A. Ganeev,[1,2,*] L. B. Elouga Bom,[1] M. C. H. Wong,[3] J.-P. Brichta,[3] V. R. Bhardwaj,[3] P. V. Redkin,[4] and T. Ozaki[1]
[1]*Centre Énergie, Matériaux et Télécommunications, Institut National de la Recherche Scientifique, 1650 Lionel-Boulet, Varennes, Québec, Canada J3X 1S2*
[2]*Institute of Electronics, Uzbekistan Academy of Sciences, Akademgorodok, 33 Dormon Yoli Street, Tashkent 100125, Uzbekistan*
[3]*Department of Physics, University of Ottawa, 150 Louis Pasteur, Ottawa, Ontario, Canada K1N 6N5*
[4]*Samarqand State University, Samarqand 703004, Uzbekistan*
(Received 1 May 2009; published 9 October 2009)

We performed systematic investigation of high-order harmonic generation from fullerene-rich laser-produced plasmas. We studied harmonic generation by varying several experimental parameters, such as the delay between the ablation and driving pulses, and divergence and polarization of the pump laser. Enhancement of harmonic yield is observed near 20 eV, which is attributed to the influence of a broadband plasmon resonance of C_{60} on the nonlinear optical response of fullerene-rich plasma. This increase in the harmonic intensity occurs despite the increased absorption by C_{60} at these wavelengths. Using simulations based on time-dependent density-functional theory, we confirm that this effect is due to the influence of collective excitations. We compare harmonic generation from fullerenes using lasers with 793 nm and 396 nm wavelengths, which show the influence of plasmon resonance on the conversion efficiency of high-order harmonics for different laser wavelengths.

DOI: 10.1103/PhysRevA.80.043808 PACS number(s): 42.65.Ky, 52.38.Mf, 78.67.Bf

I. INTRODUCTION

High-order harmonic generation (HHG) of ultrashort laser pulses is an attractive method to generate extreme ultraviolet (xuv) radiation and attosecond light pulses. Currently, various techniques are used for HHG, such as the interaction of intense laser with gases [1], with low-density laser-produced plasmas [2], and by reflecting relativistic intensity laser pulses from solid surfaces [3]. However, the brightness of such HHG sources precludes their use in various applications, such as conducting xuv nonlinear optics and spectroscopic studies.

HHG conversion efficiency can be enhanced by (a) improving the phase matching conditions [4], (b) periodically modulating the atomic density in the nonlinear medium [5], (c) exploiting the resonance of an ionic transition with a specific harmonic order [6], (d) using atomic clusters that results in increased recombination probability of the recolliding electron with the parent particle and in resonant enhancement due to expanding clustered plasma [7–10], and (e) applying surface plasmon resonances (SPRs) for low-order harmonics [11] and in large molecules and nanostructures [12]. However, the maximum achieved harmonic efficiency in the xuv range still remains relatively low (10^{-6}–10^{-5}) for atomic and ionic media.

By using particles with larger size (such as clusters of gas and metal atoms), enhancement of HHG efficiency has been observed, compared with those from media rich in single atoms or ions. Likewise, fullerenes are an attractive molecule to study HHG as they have relatively large sizes (~0.8 nm) and demonstrate broadband SPR in the xuv [$\lambda_{SPR}=60$ nm, 10 nm full width at half maximum (FWHM) [13,14]]. We have recently reported the first demonstration of HHG from fullerenes and showed an enhancement of harmonics near its SPR [15].

In this paper, we report the results of systematic studies of HHG in C_{60}-rich laser-produced plasma under different plasma conditions and laser parameters to develop further understanding of the processes previously reported. Specifically, we investigated (i) the enhancement of harmonic yield near SPR and (ii) the extension of the harmonic cutoff, using different pump wavelengths, polarization and by optimizing the time delay between prepulse and main pulse. Using simulations based on time-dependent density-functional theory (TDDFT) and on absorption and phase matching, we confirm the influence of collective excitations on enhancement of HHG near SPR. We show that the enhancement of HHG near SPR of C_{60} is independent of the pump laser wavelength.

II. EXPERIMENTAL SETUP

Experiments were performed using the 10 Hz, 10 TW beam line of the Canadian Advanced Laser Light Source at the Institut National de la Recherche Scientifique. First, plasma is created by focusing an ablation pulse (using a spherical lens, 150 mm focal length) that was split from the uncompressed Ti:sapphire laser (pulse duration $t=210$ ps, wavelength $\lambda=793$ nm) on to a target placed in vacuum. The size of the ablation beam on the target was maintained between 0.5 and 0.8 mm. The intensity of the subnanosecond ablation pulse (I_{pp}) on the target surface was varied between 2×10^{9} to 3×10^{10} W cm^{-2}. After some delay, the femtosecond driving pulse ($E=8$–25 mJ, $t=35$ fs, $\lambda=793$ nm central wavelength, 35 nm FWHM) was focused on the plasma from the orthogonal direction using an MgF_2 plano-convex lens ($f/15$, $f=680$ mm). The distance of driving beam from the target surface was maintained between 50 to 150 μm. Our experiments were performed with femtosecond main pulse intensities of up to $I_{fp}=7\times10^{14}$ W cm^{-2}, above which the HHG efficiency considerably decreased due to impeding

*rashid_ganeev@mail.ru

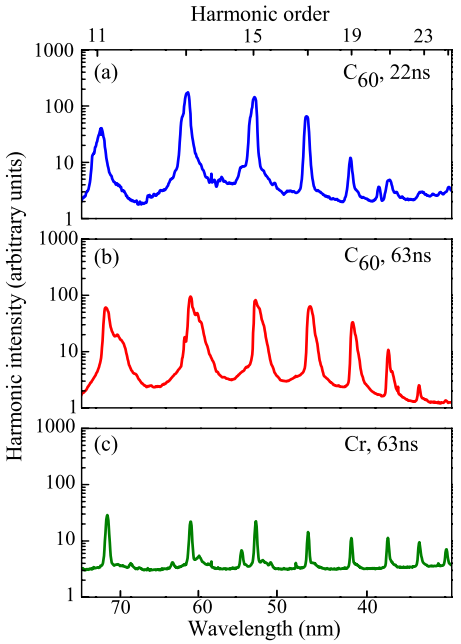

FIG. 1. (Color online) Harmonic generation observed in C_{60} plasma at (a) 22 ns and (b) 63 ns delays between the ablation pulse and driving pulse and (c) in chromium plasma.

effects in the laser plasma, such as increase in free-electron density, self-defocusing, and phase mismatch between the fundamental and harmonic waves. We also used the second harmonic of our laser as the HHG driving pulse. For these purposes, the 793 nm laser was frequency doubled in a 1 mm thick, type I KDP crystal before focusing on the plasma plume. During these experiments, the 396 nm pump was selected using UV filters. The high-order harmonics were spectrally dispersed by an xuv spectrometer with a flat-field grating (1200 lines/mm, Hitachi). The xuv spectrum was then detected by a microchannel plate and finally recorded using a charge-coupled device. Details of the experimental setup can be found elsewhere [16]. The targets used in these studies were a few-μm thick C_{60} films deposited on a glass substrate. Other targets investigated for the purpose of comparison were bulk carbon, manganese, and chromium.

III. RESULTS AND DISCUSSION

A. Influence of various experimental parameters on the HHG efficiency in fullerene plasma

In our previous studies on HHG in ablation plume of fullerene-rich targets [15], we have shown that (i) harmonics lying in the spectral range of SPR in C_{60} (20 eV) are enhanced, (ii) the harmonic yields are larger by a factor of 20–25 for 13th harmonic compared to those generated from carbon-monomer-rich plasma, and (iii) the harmonic cutoff in C_{60} is lower (19th order) than carbon but extends beyond the value (11th order) predicted by the three-step model. In the present work, we were able to improve the experimental conditions for producing ablation plume, and the laser interaction resulted in extension of the harmonic cutoff in C_{60} up to the 25th order, as shown in Fig. 1.

Figure 1 also shows harmonic spectra in C_{60} for different delays between the ablation pulse and driving pulse. HHG by ablation of bulk materials is greatly influenced by the temporal delay between the ablation pulse and driving pulse, as it alters the atomic density and plasma length in the interaction region. To study its influence, we varied the delay from 18 ns to approximately 100 ns. Our measurements showed no significant changes in the harmonic intensities in C_{60} [see Figs. 1(a) and 1(b)] for delays of 22 ns and 63 ns. Overall, the two delays produce approximately equal harmonic intensity, with some twofold increase in harmonic efficiency for the shorter delay.

However, for bulk targets such as C, Cr, and Mn, no harmonics were observed in their plasmas when we used very short delays ($\sim$6 ns), contrary to the case of C_{60}. This can be attributed to the nonoptimal plasma conditions since it requires time for the plasma to ablate on the bulk surface and expand into the area where the femtosecond beam interacts with the plasma. This can also be inferred from the lower ablation pulse intensity ($I_{pp} \sim 2 \times 10^9$ W cm^{-2}) needed for HHG from C_{60}-rich target, compared with that needed for bulk targets [$I_{pp} > 10^{10}$ W cm^{-2}]. We postulate that short delays lead to more favorable evaporation conditions and higher particle density for the cluster-rich medium compared with the monoatomic medium, thus resulting in a higher harmonic yield. In most cases of heavy bulk targets, the strong harmonics were observed using longer delays (40–70 ns). The use of light targets (B, Be, Li) showed an opposite tendency, where one can obtain effective HHG for shorter delays. The optimization is related with the presence of appropriate amount of particles at the area of fundamental laser focusing, which depends on the propagation velocity of the plasma front (see also our reply to the first remark of referee). For C_{60}, one can expect the optimization of HHG at longer delays due to the larger weight of the fullerene particles. However, one has to admit the possibility of the presence of the fragments of C_{60} in the plume, in which case, the density of the medium in the area of interaction with laser pulse becomes sufficient even for shorter delays.

An interesting feature of the fullerene harmonic spectra is that the spectral width is about three to four times broader compared with those generated in monoatom-rich plasmas (1.2 nm and 0.3 nm FWHM, respectively). For comparison, Fig. 1(c) shows the harmonic spectra from ablation of Cr. Broader width of the harmonics can be explained by self-phase modulation and chirping of the fundamental radiation propagating through the fullerene plasma. Broadening of the main beam bandwidth causes the broadening of the harmonic's bandwidth. The variation in harmonic bandwidth with delay can be explained by the higher density of the fullerene plasma for the longer delay and consequently stronger self-phase modulation of the fundamental radiation followed by broader width of harmonics. Another reason is the appearance of a larger plasma volume at longer delay, resulting in the femtosecond driving laser to propagate over a longer distance.

The intensities of the ablation pulse and driving pulse are crucial for optimizing the HHG from C_{60}. Increasing the intensity of the driving pulse did not lead to an extension of the cutoff for the fullerene plume, which is a sign of HHG satu-

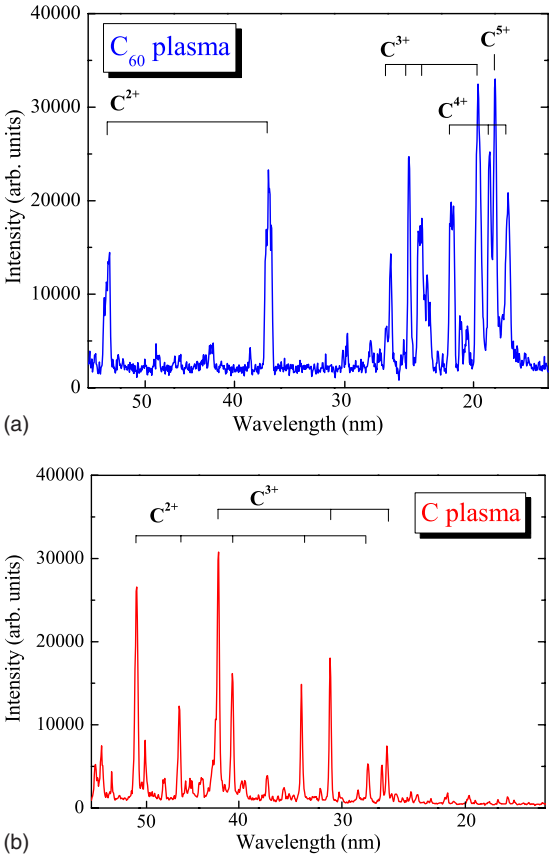

FIG. 2. (Color online) Plasma spectra of laser-ablated (a) C_{60} film and (b) C bulk target observed at high ablation pulse intensity ($I_{pp}=2\times10^{10}$ W cm^{-2}).

ration in the medium. Moreover, at relatively high femtosecond laser intensities, we observed a decrease in the harmonic output, which can be ascribed to phase mismatch as a result of higher free-electron density. A similar phenomenon is observed when the ablation pulse intensity on the surface of fullerene-rich targets is increased above the optimal value for harmonic generation. This reduction in harmonic intensity can be attributed to phenomena such as the fragmentation of fullerenes, an increase in free-electron density, and self-defocusing. At relatively strong ablation intensity for fullerene film ($I_{pp}>1\times10^{10}$ W cm^{-2}), we observed only the plasma spectrum, without any sign of harmonics as shown in Fig. 2(a).

The xuv spectra emitted by the plasma created in a vapor of C_{60} molecules have been studied by Wülker *et al.* [17]. Although the experimental conditions are different, the plasma emission spectra are comparable to that shown in Fig. 2(a). The spectra show multiple transitions in the range of 18–26 nm associated with ionized fragments of C_{60} (in particular from the C^{3+}–C^{5+}) together with the transitions near 38 and 54 nm. Contrary to fullerene plasma spectrum, carbon plasma spectrum at these conditions showed ionic transitions only from lower-charged ions as shown in Fig. 2(b). The origin of this difference was attributed to multielectron dissociative ionization of molecules as a complex dynamic sequence of events.

The stability of C_{60} molecules to ionization and fragmentation is of particular interest, especially for their application

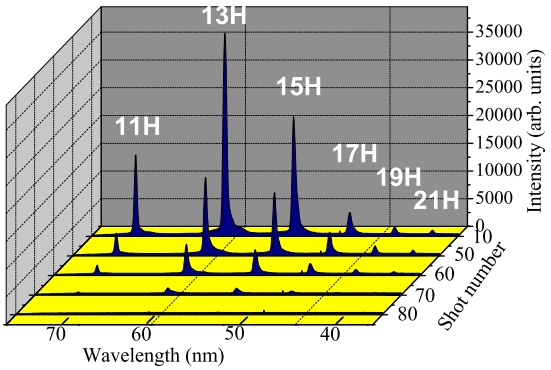

FIG. 3. (Color online) Variation in harmonic spectra after different number of laser shots on the same target position in the case of a 10-μm film.

as a medium for HHG. The structural integrity of the fullerenes ablated off the surface should be intact until the driving pulse arrives. Therefore, the ablation pulse intensity is a very sensitive parameter. At lower intensities the concentration of clusters in the ablation plume would be low, while at higher intensities one can expect fragmentation. C_{60} has demonstrated both direct and delayed ionization and fragmentation processes and is known to survive even in intense laser fields, which can be attributed to large number of internal degrees of freedom that leads to the fast diffusion of the excitation energy [18,19]. At 796 nm, multiphoton ionization is the dominant mechanism leading to the ionization of C_{60} in a strong laser field. The collective motion of π electrons of C_{60} can be excited by multiphoton process. Since the laser frequency is much smaller than the resonance frequency of π electrons, barrier suppression and multiphoton ionization are the dominant mechanisms leading to the ionization in a strong laser field.

Another important parameter that affects the stability of HHG process is the thickness of the fullerene target. We obtained stable harmonic generation with low shot-to-shot variation in harmonic intensity by moving the fullerene film deposited on the glass substrate after several laser shots. This avoids decrease in the fullerene density due to ablation of the thin film. The number of laser shots at the same target position that resulted in stable harmonic emission decreased drastically with the film thickness. For example, in a 10-μm film, the harmonic emission disappeared after 70–90 shots, as shown in Fig. 3, whereas in a 2-μm film the number of laser shots is reduced to 5–7. Like other experiments on HHG, we have also observed the influence of aperture size on the harmonic yield due to better phase matching conditions for some groups of harmonic orders.

To understand the origin of the harmonic emission in C_{60}, we investigated its dependence on the polarization of the driving pulse. This also enables to differentiate the plasma emission from the HHG process. HHG is highly sensitive to laser polarization since the trajectories of the recolliding electrons are altered significantly, thereby inhibiting the recombination process. We observed the harmonic signal to drop rapidly and disappear with ellipticity of the laser polarization. Figure 4 shows the HHG spectra for linear and circular polarizations. For circular polarization, as expected, the

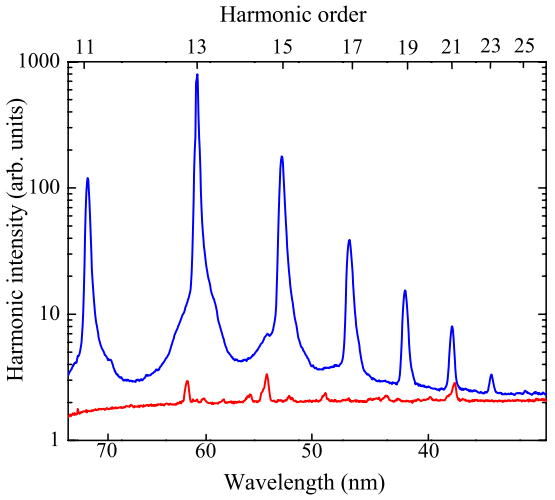

FIG. 4. (Color online) Harmonic spectra obtained in C_{60}-rich plasma, for linearly (upper curve) and circularly (bottom curve) polarized driving laser.

harmonic emission disappears and the resulting background spectrum corresponds to the plasma emission (see Fig. 2).

Does the influence of plasmon resonance on the HHG in fullerene plasma depend on the wavelength of the driving field? To address this question, we also studied the HHG using the second harmonic (396 nm, 4 mJ, 35 fs) of the driving pulse (793 nm, 30 mJ). The relatively low second-harmonic conversion efficiency did not allow us to achieve the laser intensities attained with the 793 nm fundamental laser. As a result, we were able to generate harmonics up to the ninth order of the 396 nm driving pulse, while simultaneously generating harmonics using the 793 nm laser. The harmonic generation using two driving pulses (793 nm and 396 nm) did not interfere with each other, since the two HHG processes occurred in different regions of the laser plasma, due to different focal positions of these two beams ($\sim$2 mm in the Z axis and $\sim$0.2 mm in the X axis). Here, the Z axis is the axis of propagation of the driving beam, and the X axis is the axis perpendicular to the Z axis. This axis is defined by the walk-off direction of the second harmonic with respect to the fundamental driving pulse.

Figure 5(a) shows the HHG spectrum from C_{60} fullerene optimized for the second harmonic driving pulse. The energy of the second harmonic is $\sim(1/7)$-th of fundamental. One can see the enhancement of the seventh harmonic (which is within the range of the SPR of C_{60}) compared with the fifth harmonic. This behavior is similar to that observed for the 793 nm driving pulse. For comparison, we present in Fig. 5(b) the optimized harmonics generated using the 396 nm radiation and the weak harmonics from the 793 nm radiation in manganese plasma. One can see a decrease in harmonic intensity from the Mn plume for each subsequent order, which is a common case, when one uses a nonlinear optical medium containing atomic or ionic particles. These studies confirmed that, independent of the driving pulse wavelength, the harmonics near SPR in C_{60} are always enhanced.

We did not measure the absolute value of the harmonic conversion efficiency in the plateau range. However, by using a calibration technique for harmonics from silver plasma

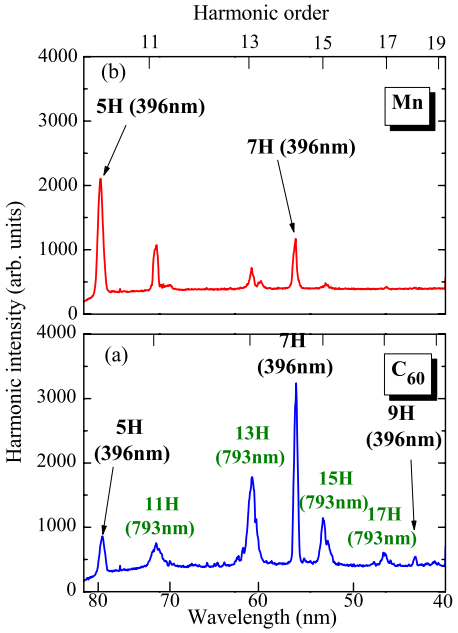

FIG. 5. (Color online) Harmonic spectra from (a) C_{60} and (b) Mn plasma, when both the 793 nm and 396 nm pulses were simultaneously focused on the laser-produced plasma.

[2], we estimate the efficiency of the 13th harmonic from fullerene plume to be above 10^{-5}.

B. Simulations of harmonic spectra

To understand the influence of the absorptive properties of surface plasmon resonance on the harmonic emission spectrum in C_{60}, we simulated the emission spectrum using approximately identical experimental parameters. The efficiency of the HHG process can be understood in terms of three length parameters. For optimum HHG, the length of the nonlinear medium L_{med} should be (a) larger than the coherence length $L_{coh}=\pi/\Delta k$, which is defined by the phase mismatch between the fundamental and harmonic fields ($\Delta k = k_q - qk_0$, where k_q and k_0 are the harmonic and fundamental wave vectors, respectively) and depends on density and ionization conditions, and (b) smaller than the absorption length of the medium $L_{abs}=1/\rho\sigma$, where ρ is the atomic density and σ is the ionization cross section. When propagating through a medium, the wave vector of light with vacuum wavelength λ is given by

$$k = \frac{2\pi n_g(\lambda)}{\lambda} \tag{1}$$

with the index of refraction, $n_g = 1 + P\delta(\lambda)$, with pressure, P, in atmospheres and a suitable gas dispersion function, $\delta(\lambda)$. In general, empirical relationships are difficult to deduce at wavelengths shorter than the ultraviolet, although calculated data can be incorporated.

For sufficiently large laser intensities, partial ionization of the gas medium occurs, resulting in a modified index of refraction.

$$n_g = 1 + (1-\eta)P\delta(\lambda) + (1-\eta)n_2 I - \eta P N_{atm} r_e \lambda^2/2\pi, \tag{2}$$

where N_{atm} is the number density at atmosphere pressure, η is the ionization fraction, and r_e is the classical radius of an

electron. The nonlinear index of refraction, n_2, is sufficiently small at this intensity that we will not consider it further. We have assumed an ionization fraction of η=0.5 for both carbon and C_{60}.

The phase mismatch between the fundamental and the qth harmonic can then be written,

$$\Delta k = \eta P N_{atm} r_e (q\lambda_0 - \lambda_q) - \frac{2\pi(1-\eta)P}{\lambda_q}[\delta(\lambda_0) - \delta(\lambda_q)]. \tag{3}$$

The number of photons in the qth harmonic per unit time and area emitted on-axis is proportional to

$$N_{out} \propto \rho^2 A_q^2 \frac{4\rho^2 L_{abs}^2}{1 + 4\pi^2 (L_{abs}^2/L_{coh}^2)} \left[1 + \exp\left(-\frac{L_{med}}{L_{abs}} \right) - 2\cos\left(\frac{\pi L_{med}}{L_{coh}} \right) \exp\left(-\frac{L_{med}}{2L_{abs}} \right) \right], \tag{4}$$

where A_q is the amplitude of the atomic response approximated to be $(1-\eta)I^3$, where I is the laser intensity [20].

The photoionization cross section of C_{60} is well known, both experimentally and theoretically. It exhibits a giant and broad plasmon resonance at ~20 eV (around the 11th, 13th, and 15th harmonics, with a bandwidth of 10 eV FWHM). We calculated the absorption length using the estimated fullerene density in the interaction region (5×10^{16} cm^{-3}) and the known photoionization cross sections. The absorption length varies from 0.8 mm (for the seventh and 17th harmonics) to 0.3 mm (for the 11th, 13th, and 15th harmonics), indicating that harmonics in the region of the plasmon resonance should be more strongly absorbed in the medium (whose length is estimated to be about 0.8–1 mm).

Due to this increased absorption in C_{60}, we expect a dip in the harmonic spectrum for the 11th–15th harmonics. Our calculations also indicate that harmonics produced in carbon vapor are not absorbed by the nonlinear medium. With an assumed medium length of 1 mm, theoretical spectra are obtained by inserting the appropriate wavelength-dependent index of refraction and dispersion data into Eqs. (3) and (4). For carbon, the index of refraction data was taken from [21] while the photoabsorption cross-section data was taken from [22]. For C_{60}, the photoabsorption cross-section data was taken from [23]. As we did not have access to reliable index of refraction data for C_{60}, we have simply used a wavelength-dependent index of refraction that scales with the photoabsorption cross section.

Figure 6 shows the calculated harmonic spectra for C_{60} and carbon plasmas by considering only absorption (squares and circles, respectively) and by including both absorption and dispersion (up and down triangles, respectively). In carbon vapor, the influence of absorption on the harmonic yield is negligible and as a result the overall harmonic spectrum is determined by dispersion. The harmonic yield decreases with increasing order as it becomes difficult to phase match higher orders.

In C_{60}, absorption of harmonics by the nonlinear medium is dominant due to large photoabsorption cross sections. The effect of dispersion seems to only lower the HHG efficiency

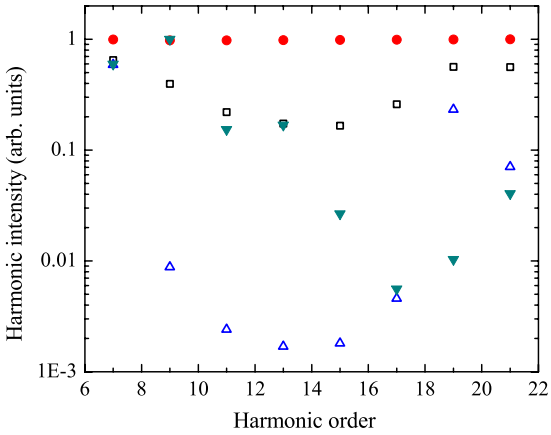

FIG. 6. (Color online) The theoretical harmonic spectrum for C_{60}, considering absorption only (squares) and a combination of absorption and dispersion (upward triangles). When dispersion is included, the predicted harmonic signal is quite small. The spectra for carbon are included for comparison. Identical results are obtained when using the absorption only model (circles) and absorption and dispersion (downward triangles).

but does not affect the overall shape of the spectrum. As a result one expects the harmonic yield to decrease considerably near the surface plasmon resonance, if one does not consider the nonlinear optical influence of this resonance on the harmonic efficiency in this medium. On the contrary, in our experiment, we observed a considerable enhancement of these harmonics in the fullerene-rich plume (Figs. 1, 3, and 4). This is a signature of multielectron dynamics in a complex molecule such as C_{60} and has no atomic analog.

To understand the origin of enhancement of harmonic yield near SPR, we theoretically investigated the interaction of monatomic carbon and fullerene C_{60} molecule with a strong laser pulse by means of the TDDFT [24]. In the TDDFT approach, the many-body time-dependent wave function is replaced by the time-dependent density $n(r,t)$, which is a simple function of the three-dimensional vector r. $n(r,t)$ is obtained with the help of a fictitious system of noninteracting electrons by solving the time-dependent Kohn-Sham equations,

$$i\frac{\partial}{\partial t}\varphi_i(r,t) = \left[-\frac{\nabla^2}{2} + \upsilon_{\mathrm{KS}}(r,t) \right] \varphi_i(r,t). \tag{5}$$

These are one-particle equations, so it is possible to treat large systems such as fullerenes. The density of the interacting system is obtained from the time-dependent Kohn-Sham orbitals,

$$n(r,t) = \sum_{i}^{occ} |\varphi_i(r,t)|^2, \tag{6}$$

$$\upsilon_{\mathrm{KS}}(r,t) = \upsilon_{ext}(r,t) + \upsilon_{\mathrm{Hartree}}(r,t) + \upsilon_{xc}(r,t). \tag{7}$$

Here $\upsilon_{ext}(r,t)$ is the external potential (laser field), $\upsilon_{\mathrm{Hartree}}(r,t)$ accounts for the classical electrostatic interaction between the electrons,

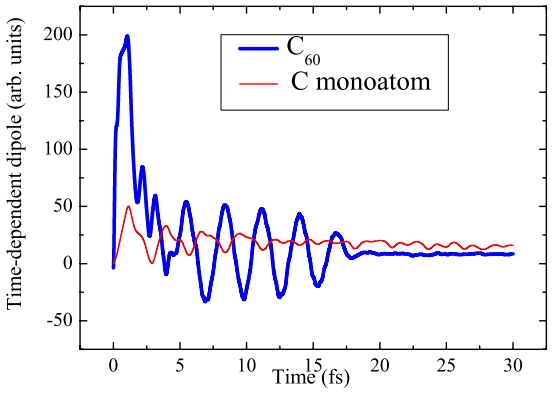

FIG. 7. (Color online) Calculated time-dependent dipoles of C_{60} and carbon monoatom.

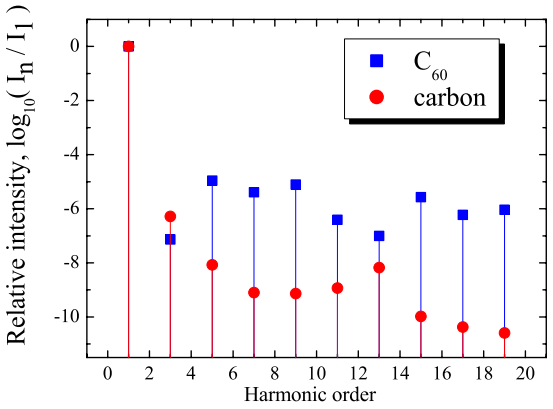

FIG. 8. (Color online) Calculated relative intensities of harmonics generated from neutral carbon monoatom and C_{60} fullerene molecule.

$$v_{\text{Hartree}}(r,t) = \int d^3r' \frac{n(r,t)}{|r-r'|}. \tag{8}$$

We treated the exchange and correlation within the so-called adiabatic local density approximation (ALDA) assuming that the potential is the time-independent *xc* potential evaluated at the time-dependent density,

$$v_{xc}^{\text{adiabatic}}(r,t) = \tilde{v}_{xc}[n](r)|_{n=n(t)}. \tag{9}$$

For all calculations we used the OCTOPUS code [25] with norm-conserving nonlocal Troullier-Martins pseudopotentials [26], Slater exchange, Perdew and Zunger correlation functionals [27], and grid spacing of 0.6 Å for parallelepiped box of $8\times8\times60$ Å. Figure 7 shows the time-dependent dipoles resulting from the interaction of neutral monatomic carbon and C_{60} molecule that is polarized in the *X*-axis direction parallel to the polarization direction of the electromagnetic wave with photon energy of 1.5 eV and maximum intensity of 4.8×10^{14} W cm^{-2} during 30 fs. The time step of the integration was 0.001 fs. The ions were treated as static, and the fragmentation of C_{60} molecule was not investigated. The geometry of C_{60} fullerene was obtained with the PCGAMESS package [28–30]. PCGAMESS is an *ab initio* quantum chemistry software package, which was used to obtain the coordinates of the carbon atoms in the C_{60} molecule. One can see from Fig. 7 that, for a C_{60} molecule, the maximum dipole is 4 times larger than in monatomic carbon, which corresponds to a 16-fold enhancement of the nonlinear optical response of the generated harmonic field. In both cases the time-dependent dipole is fading. Since we use nonfading wave, the only reason for this is the ionization, which makes any contributions beyond 20 fs negligible.

We analyzed the relative harmonic intensities calculated for C_{60} and carbon (Fig. 8). A significant increase in HHG efficiency for C_{60} molecule can be attributed to additional oscillation of the time-dependent dipole in the C_{60} molecule. This can be a sign of an induced collective plasmonlike response of the molecule to external field. At the same time the cutoff for the carbon atom is higher than that for a fullerene molecule. The treatment of very high harmonics with ALDA can become inaccurate because this approximation suffers from an exponential cutoff of the exchange and correlation potential. The effects of correlation for lower harmonics are nevertheless conserved, so a collective oscillation can be responsible for the relative increase in the time-dependent dipole and, respectively, HHG conversion efficiency observed in plasma of fullerene molecules.

The software used in these HHG investigations is a real-time real-space method, which means any wave function must be presented on a numerical grid, that is, only in certain points in real space. As the computational effort grows strongly with the number of grid points, the grid (points, where the wave function of a system is presented) was chosen so that the maximum harmonic energy could be not greater than the cutoff observed. In addition, we are in general not sure whether the remaining high-energy part is not simply artifacts and noises from discrete Fourier transforms. So these cutoff positions should be considered with care. All the data on HHG presented are also not simple density-functional theory-based calculations but a filtered variant of this chosen in assumption that some (not all) Gauss-broadened multiplets of main radiation should be presented in the spectrum. As the spectrum itself is based on the density-functional theory, it also suffers from the problems of density functions for finite intervals. Namely, to resolve a 10^{-6} of the pump's intensity for a perfect sine pulse superposition, we need at least 15 periods of it. No one can exactly say what happens if we consider less time intervals and intensities. In general, this computation suffers from numerical inaccuracies.

Below we address the mechanism of plasma formation above the target surface. The creation of nonlinear medium above the target surface is not based on the simple heating of the target surface and steady-state processes of melting, evaporation, and spreading of the particles with the velocities defined from the thermodynamic relations. This relation refers to cw heating. In this case the velocity of the C_{60} molecule at 1000 K is in the range of 1.5×10^2 m s^{-1}. During the first few nanoseconds ($\sim$10 ns) the fullerene molecules will move only 1.5 μm above the surface. If one assumes that plasma creation by short laser pulse is defined by this

slow process, then no harmonics at all should be observed in such experimental configuration for any target. For example, laser ablation of silver creates very efficient "nonlinear" plasma, which allows generating extremely strong high harmonics when the femtosecond pulse propagates 100 μm above the target surface. The same can be said about any other targets, which was documented in multiple studies during last decade (see for example [2,31,32]). However, when one uses the above relation, the velocity of Ag neutral atoms and ions can be about 5.5×10^{2} m s^{-1}. During the first 30 ns they travel only 16 μm away from the target surface, which is quite insufficient to reach the axis of the driving pulse.

This contradiction is explained by another model of creation of the cloud of particles, namely, plasma explosion during ablation of the targets. The dynamics of plasma front propagation during laser ablation is studied by few groups (for example [33], and references therein). The dynamics of plasma formation and spreading can be analyzed by the shadowgram technique. The radiation intensity used in this technique can be varied in a wide range (from 10^{6} to 10^{19} W cm^{-2}). Numerical analysis of the generation of such plasmas for the case of single-pulse interaction with the target surface was performed in [34]. Previously, the dynamics of the spatial characteristics of laser plasmas generated from B and Mo targets, measured using the shadowgraphs of the plasma blocks, was reported in [35]. For heavy targets (Mo), the plasma front spreads with the velocity of 6×10^{4} m s^{-1}. For example, the plasma front reaches 130 μm distance from the target after few nanoseconds (not few hundreds ns, as is estimated if we assume steady-state expansion of the plasma particle cloud). Obviously, the formation of "optimal" plasma is not restricted by appearance of the plasma front in the area of femtosecond pulse. One can wait until the density of the particles becomes sufficient for efficient HHG, while the free-electron concentration remains below the level when the impeding processes prevail over the harmonic generation.

We do not insist that, at initial stages of plasma front formation and propagation through the area of propagation of the femtosecond radiation, the components of plasma consist only on the intact fullerenes. To make such a conclusion one should analyze the plasma dynamics using the time-of-flight spectroscopy. However, the above explanation seems reasonable to admit that the ability of particles to be at the right time on the right place is based on the fast processes of plasma explosion rather than slow steady-state process of target heating.

The higher harmonic yield in a highly polarizable molecule like C_{60} compared to an atom could simply be due to enhanced recombination cross sections resulting from its larger spatial extent. Also the delocalized electron distribution can lead to large induced dipole as shown above. The harmonic efficiency depends on the square of the dipole matrix. While these explain higher harmonic yield in C_{60} in general they do provide insight into why only harmonics near SPR are enhanced.

Higher cutoff observed in our experiments could be due to (i) the contribution of C_{60} ions to HHG process—laser ablation at prepulse intensities used in the experiment is known to lead to soft ionization identical to matrix-assisted laser desorption/ionization—and (ii) multiphoton excitation of surface plasmon (20 eV) by the incident laser field (1.55 eV). If ionization starts from a plasmon state and the electron returns to the ground state upon recombination, the plasmon energy is converted into photon energy extending the cutoff [36]. (iii) Recombination into orbitals, other than the highest occupied molecular orbital of C_{60}, with higher ionization potentials [37] can result in extension of cutoff.

High harmonics in C_{60} or in any complex multielectron system will have two contributions—the usual harmonics generation process and the physical mechanisms that lead to enhancement of harmonics (9th–15th in C_{60}) around the frequencies at which the system displays collective electron oscillations (20 eV in C_{60} with $\sim$10 eV FWHM). Plasmon excitation under two different scenarios can lead to enhancement of high harmonics. (i) The recolliding electron excites the plasmon upon recombination, which then decays by emitting photons. This leads to enhancement of the harmonics in the vicinity of plasmon resonance [37]. Such a mechanism would be wavelength dependent. It was shown that at longer wavelengths the HHG spectrum resembles that of atomic systems. (ii) The laser field directly excites the surface plasmon through multiphoton process, which then decays back by emitting high-energy photons [36]. Similar bound-bound transitions were theoretically shown to exist [38] in C_{60}. Such a mechanism will be independent of recollision process and can be revealed by ellipticity measurements. Recent theoretical calculations of the HHG in C_{60} using a simple analytical theory, which predicts that the recollision-induced excitation of collective modes should dominate over the "usual" harmonic generation yield at 800 nm wavelength, have confirmed the observed growth of harmonic yield in the vicinity of their SPR [31]. Further studies on isolated C_{60} molecules should shed light on the mechanisms responsible for enhancements of the harmonic yield.

IV. CONCLUSIONS

We presented results of systematic studies of the HHG in C_{60}-rich laser plasma. We analyzed the harmonics at different delays between the ablation pulse and driving pulse. We also studied the HHG at various divergence and polarization conditions of the driving laser. We further investigated the enhancement of the harmonic yield near 20 eV and showed that this process is attributed to the influence of a broadband plasmon resonance of C_{60} on the nonlinear optical response of fullerene-rich plasma. This intensity enhancement of fullerene harmonics is distinct, since absorption by C_{60} in this wavelength range should be pronounced. We compared the HHG using both the fullerene-rich plumes and different single-atom plasma species. These studies showed a significant broadening of harmonic lines for C_{60}-rich plasma, and confirmed a greater than ten-fold enhancement of harmonic yield in the fullerenes, compared with the monoatomic media under equivalent experimental conditions. Simulations using time-dependent density-functional theory confirmed the influence of collective excitations on this effect. Comparison of harmonic generation in fullerenes using 793 nm and 396

nm pulses showed the enhancement of high-order harmonics of both these driving pulses near the C_{60} SPR. These studies have shown that C_{60} is not only a promising material for HHG, but may also present an opportunity to develop HHG into a tool to probe electronic structure.

ACKNOWLEDGMENT

R.A.G. gratefully acknowledges the support from the Natural Sciences and Engineering Research Council of Canada to carry out this work.

[1] S. Kazamias, D. Douillet, F. Weihe, C. Valentin, A. Rousse, S. Sebban, G. Grillon, F. Auge, D. Hulin, and P. Balcou, Phys. Rev. Lett. **90**, 193901 (2003).
[2] R. A. Ganeev, J. Phys. B **40**, R213 (2007).
[3] P. A. Norreys, M. Zepf, S. Moustaizis, A. P. Fews, J. Zhang, P. Lee, M. Bakarezos, C. N. Danson, A. Dyson, P. Gibbon, P. Loukakos, D. Neely, F. N. Walsh, J. S. Wark, and A. E. Dangor, Phys. Rev. Lett. **76**, 1832 (1996).
[4] E. A. Gibson, A. Paul, N. Wagner, R. Tobey, D. Gaudiosi, S. Backus, I. P. Christov, A. Aquila, E. M. Gullikson, D. T. Attwood, M. M. Murnane, and H. C. Kapteyn, Science **302**, 95 (2003).
[5] J. Seres, V. S. Yakovlev, E. Seres, Ch. Streli, P. Wobrauschek, Ch. Spielmann, and F. Krause, Nat. Phys. **3**, 878 (2007).
[6] R. A. Ganeev, H. Singhal, P. A. Naik, V. Arora, U. Chakravarty, J. A. Chakera, R. A. Khan, I. A. Kulagin, P. V. Redkin, M. Raghuramaiah, and P. D. Gupta, Phys. Rev. A **74**, 063824 (2006).
[7] T. D. Donnelly, T. Ditmire, K. Neuman, M. D. Perry, and R. W. Falcone, Phys. Rev. Lett. **76**, 2472 (1996).
[8] J. W. G. Tisch, T. Ditmire, D. J. Fraser, N. Hay, M. B. Mason, E. Springate, J. P. Marangos, and M. H. R. Hutchinson, J. Phys. B **30**, L709 (1997).
[9] R. A. Ganeev, M. Suzuki, M. Baba, M. Ichihara, and H. Kuroda, J. Phys. B **41**, 045603 (2008).
[10] R. A. Ganeev, M. Suzuki, M. Baba, M. Ichihara, and H. Kuroda, J. Appl. Phys. **103**, 063102 (2008).
[11] B. Shim, G. Hays, R. Zgadzaj, T. Ditmire, and M. C. Downer, Phys. Rev. Lett. **98**, 123902 (2007).
[12] S. Kim, J. Jin, Y.-J. Kim, I.-Y. Park, Y. Kim, and S.-W. Kim, Nature (London) **453**, 757 (2008).
[13] R. G. Polozkov, V. K. Ivanov, and A. V. Solov'yov, J. Phys. B **38**, 4341 (2005).
[14] S. Hunsche, T. Starczewski, A. l'Huillier, A. Persson, C.-G. Wahlström, H. B. van Linden van den Heuvell, and S. Svanberg, Phys. Rev. Lett. **77**, 1966 (1996).
[15] R. A. Ganeev, L. B. Elouga Bom, J. Abdul-Hadi, M. C. H. Wong, J. P. Brichta, V. R. Bhardwaj, and T. Ozaki, Phys. Rev. Lett. **102**, 013903 (2009).
[16] R. A. Ganeev, L. B. Elouga Bom, J.-C. Kieffer, M. Suzuki, H. Kuroda, and T. Ozaki, Phys. Rev. A **76**, 023831 (2007).
[17] C. Wülker, W. Theobald, D. Ouw, F. P. Schäfer, and B. N. Chichkow, Opt. Commun. **112**, 21 (1994).
[18] I. Shchatsinin, T. Laarmann, N. Zhavoronkov, C. P. Schulz, and I. V. Hertel, J. Chem. Phys. **129**, 204308 (2008).
[19] V. R. Bhardwaj, P. B. Corkum, and D. M. Rayner, Phys. Rev. Lett. **91**, 203004 (2003).
[20] E. Constant, D. Garzella, P. Breger, E. Mével, C. Dorrer, C. Le Blanc, F. Salin, and P. Agostini, Phys. Rev. Lett. **82**, 1668 (1999).
[21] D. L. Windt, W. C. Cash, Jr., M. Scott, P. Arendt, B. Newnam, R. F. Fisher, A. B. Swartzlander, P. Z. Takacs, and J. M. Pinneo, Appl. Opt. **27**, 279 (1988).
[22] B. L. Henke, E. M. Gullikson, and J. C. Davis, At. Data Nucl. Data Tables **54**, 181 (1993).
[23] T. Mori, J. Kou, Y. Haruyama, Y. Kubozono, and K. Mitsuke, J. Electron Spectrosc. Relat. Phenom. **144-147**, 243 (2005).
[24] E. Runge and E. K. U. Gross, Phys. Rev. Lett. **52**, 997 (1984).
[25] M. A. L. Marques, A. Castro, G. F. Bertsch, and A. Rubio, Comput. Phys. Commun. **151**, 60 (2003).
[26] N. Troullier and J. L. Martins, Phys. Rev. B **43**, 1993 (1991).
[27] J. P. Perdew and A. Zunger, Phys. Rev. B **23**, 5048 (1981).
[28] M. W. Schmidt, K. K. Baldridge, J. A. Boatz, S. T. Elbert, M. S. Gordon, J. H. Jensen, S. Koseki, N. Matsunaga, K. A. Nguyen, S. J. Su, T. L. Windus, M. Dupuis, and J. A. Montgomery, J. Comput. Chem. **14**, 1347 (1993).
[29] A. V. Nemukhin, B. L. Grigorenko, and A. A. Granovsky, Moscow Univ. Chem. **45**, 75 (2004).
[30] R. A. Ganeev and P. V. Redkin, Opt. Commun. **281**, 4126 (2008).
[31] S. Kubodera, Y. Nagata, Y. Akiyama, K. Midorikawa, M. Obara, H. Tashiro, and K. Toyoda, Phys. Rev. A **48**, 4576 (1993).
[32] C.-G. Wahlström, S. Borgström, J. Larsson, and S.-G. Pettersson, Phys. Rev. A **51**, 585 (1995).
[33] B. Rus *et al.*, Phys. Rev. A **56**, 4229 (1997).
[34] H. Hora, *Plasmas at High Temperature and Density* (Springer, Heidelberg, 1991).
[35] R. A. Ganeev, M. Suzuki, M. Baba, and H. Kuroda, Opt. Spectrosc. **99**, 1000 (2005).
[36] J. Zanghellini, Ch. Jungreuthmayer, and T. Brabec, J. Phys. B **39**, 709 (2006).
[37] M. Ruggenthaler, S. V. Popruzhenko, and D. Bauer, Phys. Rev. A **78**, 033413 (2008).
[38] G. P. Zhang, Phys. Rev. Lett. **95**, 047401 (2005).